

Cooling and heating the intracluster medium in hydrodynamical simulations

L. Tornatore,^{1★} S. Borgani,^{1★} V. Springel,^{2★} F. Matteucci,^{1★}
N. Menci^{3★} and G. Murante^{4★}

¹*Dipartimento di Astronomia dell'Università di Trieste, via Tiepolo 11, I-34131 Trieste, Italy*

²*Max-Planck-Institut für Astrophysik, Karl-Schwarzschild Strasse 1, Garching bei München, Germany*

³*INAF, Osservatorio Astronomico di Roma, via dell'Osservatorio, I-00040 Monteporzio, Italy*

⁴*INAF, Osservatorio Astronomico di Torino, Strada Osservatorio 20, Pino Torinese, I-10025 Italy*

Accepted 2003 March 10. Received 2003 March 10; in original form 2002 December 20

ABSTRACT

We discuss tree+SPH (smoothed-particle hydrodynamics) simulations of galaxy clusters and groups, aimed at studying the effect of cooling and non-gravitational heating on observable properties of the intracluster medium (ICM). We simulate at high resolution four group- and cluster-sized haloes, with virial masses in the range $(0.2\text{--}4) \times 10^{14} M_{\odot}$, extracted from a cosmological simulation of a flat Λ -cold dark matter model. We discuss the effects of using different SPH implementations and show that high resolution is mandatory to correctly follow the cooling pattern of the ICM. Our recipes for non-gravitational heating release energy to the gas either in an impulsive way, at some heating redshift, or by modulating the heating as a function of redshift according to the star formation history predicted by a semi-analytic model of galaxy formation. Our simulations demonstrate that cooling and non-gravitational heating exhibit a rather complex interplay in determining the properties of the ICM: results on the amount of star formation and on the X-ray properties are sensitive not only to the amount of heating energy, but also depend on the redshift at which it is assigned to gas particles. All of our heating schemes that correctly reproduce the X-ray scaling properties of clusters and groups do not succeed in reducing the fraction of collapsed gas below a level of 20 (30) per cent at the cluster (group) scale, which appears to be in excess of observational constraints. Finally, gas compression in cooling cluster regions causes an increase of the temperature and a steepening of the temperature profiles, independent of the presence of non-gravitational heating processes. This is inconsistent with recent observational evidence for a decrease of gas temperature towards the centre of relaxed clusters. Provided these discrepancies persist even for a more refined modelling of energy feedback from supernova or active galactic nuclei, they may indicate that some basic physical process is still missing in hydrodynamical simulations.

Key words: hydrodynamics – methods: numerical – galaxies: clusters: general – cosmology: theory – X-ray: galaxies: clusters.

1 INTRODUCTION

The simplest picture to describe the thermal properties of the intracluster medium (ICM) is based on the assumption that gas heating occurs only by the action of gravitational processes, such as adiabatic compression from gravitational collapse, and by hydrodynamical shocks from supersonic accretion (Kaiser 1986). Since

gravity does not have characteristic scales, this model predicts that galaxy systems of different mass should look like scaled versions of each other. Under the assumptions of thermal bremsstrahlung emissivity and hydrostatic equilibrium, this model provides precise predictions for X-ray scaling properties of galaxy systems: (i) $L_X \propto T^2(1+z)^{3/2}$ for the shape and evolution of the relation between X-ray luminosity and gas temperature; (ii) $S \propto T(1+z)^{-2}$ for the entropy–temperature relation, where $S = T/n_e^2$ is the gas entropy and n_e is the electron number density; (iii) $M \propto T^{3/2}$ for the relation between total cluster virial mass and temperature, with normalization determined by the parameter $\beta = \mu m_p \sigma_v^2 / k_B T$ ($\mu = 0.59$ is the mean molecular weight for the primordial composition,

★E-mail: tornatore@ts.astro.it (LT); borgani@ts.astro.it (SB); matteucci@ts.astro.it (FM); volker@mpa-garching.mpg.de (VS); menci@comamporzio.astro.it (NM); giuseppe@to.astro.it (GM)

m_p is the proton mass and σ_v is the line-of-sight velocity dispersion). Numerical simulations that only include gravitational heating showed that $\beta \simeq 1$ –1.3 (e.g. Navarro, Frenk & White 1995; Evrard, Metzler & Navarro 1996; Bryan & Norman 1998; Eke, Navarro & Frenk 1998b; Borgani et al. 2002, BGW hereafter).

A number of observational facts demonstrate that this picture is too simplistic, thus calling for the consideration of extra physics in the description of the ICM. The L_X – T relation is found to be steeper than predicted, with $L_X \propto T^3$ at $T_X > 2$ keV (e.g. White, Jones & Forman 1997; Markevitch 1998; Arnaud & Evrard 1999; Ettori, De Grandi & Molendi 2002) possibly approaching the self-similar scaling only for the hottest systems with $T \gtrsim 8$ keV (Allen & Fabian 1998). Evidence also emerged for this relation to further steepen for colder groups, $T \lesssim 1$ keV (e.g. Ponman et al. 1996; Helsdon & Ponman 2000; Mulchaey 2000). Furthermore, no evidence for a strong positive evolution of the L_X – T relation has been found to date out to $z \sim 1$ (e.g. Mushotzky & Scharf 1997; Reichart et al. 1999; Fairley et al. 2000; Borgani et al. 2001a; Holden et al. 2002; Novicki, Sornig & Henry 2002; cf. also Vikhlinin et al. 2002). As for the S – T relation, Ponman, Cannon & Navarro (1999) found from *ROSAT* and *ASCA* data an excess of entropy within the central regions of $T \lesssim 2$ keV systems (see also Lloyd-Davies, Ponman & Cannon 2000; Finoguenov et al. 2002), possibly approaching the value $S \sim 100$ keV cm² for the coldest groups. Finally, a series of evidence, based on *ASCA* (e.g. Horner, Mushotzky & Scharf 1999; Nevalainen, Markevitch & Forman 2000; Finoguenov et al. 2001b), *Beppo-SAX* (Ettori et al. 2002) and *Chandra* (Allen, Schmidt & Fabian 2001) data, shows that the observed M – T relation has a ~ 40 per cent lower normalization than predicted by simulations that only include gravitational heating.

In an attempt to interpret these data, theoreticians are currently following two alternative routes, based either on introducing non-gravitational heating of the ICM or on alluding to the effects of radiative cooling.

An episode of non-gravitational heating, occurring before or during the gravitational collapse, has the effect of increasing the entropy of the gas, preventing it from reaching high densities in the central cluster regions and suppressing its X-ray emissivity (e.g. Evrard & Henry 1991; Kaiser 1991; Bower 1997). For a fixed amount of specific heating, the effect is larger for poorer systems, i.e. when the extra energy per gas particle is comparable to the halo virial temperature. This produces both an excess entropy and a steeper L_X – T relation (e.g. Cavaliere, Menci & Tozzi 1998; Balogh, Babul & Patton 1999; Tozzi & Norman 2001). Arguments based on semi-analytical work (e.g. Tozzi & Norman 2001) and numerical simulations (Bialek, Evrard & Mohr 2001; Brighenti & Mathews 2001; Borgani et al. 2001b, 2002) suggest that a specific heating energy of $E_h \sim 1$ keV particle^{−1} or, equivalently, a pre-collapse entropy floor of $S \sim 100$ keV cm², can account for the observed X-ray properties of galaxy systems (cf. also Babul et al. 2002 and Finoguenov et al. 2002a for arguments suggesting a stronger pre-heating). Yet the origin for this energy has still to be determined. Energy release from supernovae (SNe) feedback has been advocated as a possibility (e.g. Bower et al. 2001; Menci & Cavaliere 2000). Using the abundance of heavy elements of the ICM as a diagnostic for the past history of star formation within clusters (e.g. Renzini 1997; Kravtsov & Yepes 2000; Pipino et al. 2002; Valdarnini 2002), a number of studies concluded that SNe may fall short in providing the required extra energy budget (cf. also Finoguenov, Arnaud & David 2001a). The other obvious candidate is represented by energy from active galactic nuclei (AGN) (e.g. Valageas & Silk 1999; Wu, Fabian & Nulsen 2000; McNamara et al. 2000; Nath & Roychowdhury 2002;

Cavaliere, Lapi & Menci 2002). In this case, the large amount of energy that is available requires some degree of tuning of the mechanisms responsible for its conversion into thermal energy of the gas. While a suitable amount of non-gravitational heating can account for the observed L_X – T relation and entropy excess, the M – T relation is only marginally affected by extra heating (e.g. BGW), thus leaving the discrepancy between the observed and the predicted relation unresolved.

As for cooling, its effect is to selectively remove those low-entropy particles from the diffuse X-ray-emitting phase that have cooling times shorter than the Hubble time (e.g. Voit et al. 2002; Wu & Xue 2002). Conversion of cooled gas into collisionless stars decreases the central gas density and, at the same time, the resulting lack of pressure support causes higher-entropy shocked gas to flow in from the outskirts of the cluster or group. As a result, the X-ray luminosity is suppressed, while the entropy increases, much like in a pre-heating scenario (Pearce et al. 2001; Muanwong et al. 2002; Davé, Katz & Weinberg 2002). However, by its nature, cooling is known to be a runaway process: cooling causes gas to be accumulated into dense structures, and the efficiency of cooling increases with gas density. As a result, most simulations consistently predict a significant fraction of gas to be converted into cold ‘stars’, $f_{\text{cold}} \gtrsim 30$ per cent (e.g. Sugimoto & Ostriker 1998; Lewis et al. 2000; Yoshida et al. 2002; BGW), while observations indicate a considerably lower value of $f_{\text{cold}} \lesssim 10$ per cent (e.g. Balogh et al. 2001; Wu & Xue 2002).

This suggests that in real clusters some source of extra heating is increasing the entropy of the gas, preventing overcooling. Voit et al. (2002) have developed a semi-analytical approach to derive X-ray observable properties of the ICM in the presence of both cooling and extra heating. Based on this approach, these authors found that cooling and a modest amount of extra heating are able to account for basically all the X-ray ICM observables. Oh & Benson (2002) pointed out that pre-heating is needed to increase the cooling time and prevent overcooling, by suppressing the gas supply to galaxies (see also Finoguenov et al. 2002). It is, however, clear that, as for any analytical approach, suitable assumptions and approximations are needed to choose criteria for removing cooled gas from the hot diffuse phase, and to follow the complex dynamics of cooling/heating of the gas during the process of cluster formation.

Muanwong et al. (2002) and Kay, Thomas & Theuns (2002) used hydrodynamical simulations within a cosmological box to study the interplay of gas cooling and a few prescriptions for non-gravitational heating. As a general result, they found that increasing the heating can suppress the amount of cooled gas. While the choice of simulating a whole cosmological box has the advantage of providing large statistics of groups and clusters, it also severely limits the available mass and force resolution. On the other hand, by the very nature of cooling, increasing the mass resolution allows one to follow the formation of smaller haloes at progressively larger redshift, where cooling and, potentially, star formation are particularly efficient. Consequently, unless very high-mass resolution is achieved, cooling in simulations can be significantly underestimated (e.g. Balogh et al. 2001).

In this paper, we follow the alternative approach of simulating at very high resolution a limited number of group- and cluster-sized haloes selected from a cosmological box, and we widen the range of possible patterns explored for non-gravitational heating (see also BGW). While this limits our ability to precisely calibrate the shape and scatter of X-ray scaling relations, we are able to increase the resolution in the most interesting regions of the gas distribution. Indeed, the simulations presented in this paper are among the

highest-resolution attempts realized so far to follow the structure of gas cooling within groups and clusters in the presence of a variety of schemes for extra gas heating. Furthermore, we also investigate how the cooling efficiency depends both on numerical resolution and on details of the smoothed-particle hydrodynamics (SPH) implementation.

The structure of this paper is as follows. After providing a short description of the code, in Section 2 we present the procedure for simulating individual haloes at high resolution and discuss the main characteristics of the four selected haloes. In Section 3, we discuss the results on the cold fraction. Here we will concentrate on showing how this fraction depends on the numerical resolution, the integration scheme and the removal of cold dense particles from the SPH computation (star formation). Finally, we present the adopted schemes for non-gravitational gas heating and discuss their impact on the resulting cold fraction and pattern of star formation. In Section 4, we present the predictions on X-ray properties of clusters and groups from our simulations, namely the entropy–temperature, the luminosity–temperature and the mass–temperature relations. Finally, we discuss our main results and draw conclusions in Section 5.

2 THE SIMULATIONS

2.1 The code

Our simulations are realized using GADGET, <http://www.mpa-garching.mpg.de/gadget> a parallel tree N -body/SPH code (Springel, Yoshida & White 2001), with fully adaptive time-step integration. Gas cooling in the SPH part of the code is implemented following Katz, Weinberg & Hernquist (1996, KWH hereafter). Specifically, the abundances of ionic species are computed by assuming collisional equilibrium for a gas of primordial composition (mass fraction $X = 0.76$ for hydrogen and $1 - X = 0.24$ for helium). Since we do not follow metal production from star formation, we do not include the effect of metals on the cooling function. We include the effect of a time-dependent uniform ultraviolet background (e.g. Haardt & Madau 1996), although its effect is only very small for the massive objects we focus on in this study. We set the number of neighbours for SPH computations to 32, allowing the SPH smoothing length to drop at most to the value of the gravitational softening length of the gas particles.

2.2 The simulated structures

We simulate four haloes at high resolution, which are extracted from a low-resolution dark-matter- (DM-) only simulation within a box of $70 h^{-1}$ Mpc on a side, for a cosmological model with $\Omega_m = 0.3$, $\Omega_\Lambda = 0.7$, Hubble constant $H_0 = 70 \text{ km s}^{-1} \text{ Mpc}^{-1}$ and normalization $\sigma_8 = 0.8$, consistent with recent determinations of the number density of nearby clusters (Pierpaoli et al. 2002 and references therein). As for the baryon content, we assume $\Omega_{\text{bar}} = 0.019 h^{-2}$ (e.g. Burles & Tytler 1998). This choice of Ω_{bar} corresponds to $f_{\text{bar}} \simeq 0.13$ for the cosmic baryon fraction, which, for the assumed cosmology, is consistent with the value measured from cluster observations (e.g. Ettori 2002 and references therein).

The most massive halo we selected corresponds to a Virgo-like cluster, with virial mass of about $4 \times 10^{14} M_\odot$ (as usual, we call ‘virial’ the mass within the radius encompassing the virial overdensity computed for the simulated cosmology; e.g. Eke et al. 1998a). This turns out to be the most massive system extracted from the simulation box. In the following, we will refer to this system as the

Table 1. Physical characteristics and numerical parameters of the simulated haloes in the HR runs. Column 2, total mass within the virial radius at $z = 0$ ($10^{13} M_\odot$); column 3, virial radius (Mpc); column 4, total mass within R_{500} ; column 5, radius containing an average density $\bar{\rho} = 500\rho_{\text{crit}}$. Column 6, number of gas particles within R_{vir} ; column 7, Plummer-equivalent softening parameter at $z = 0$ (h^{-1} kpc).

| Run | M_{vir} | R_{vir} | M_{500} | R_{500} | N_{gas} | ϵ |
|---------|------------------|------------------|-----------|-----------|------------------|------------|
| Cluster | 39.4 | 1.90 | 23.3 | 0.94 | 1.5e5 | 5.0 |
| Group 1 | 5.98 | 1.01 | 3.43 | 0.49 | 1.8e5 | 2.5 |
| Group 2 | 2.52 | 0.76 | 1.60 | 0.38 | 7.8e4 | 2.5 |
| Group 3 | 2.35 | 0.74 | 1.35 | 0.36 | 7.1e4 | 2.5 |

‘Virgo’ cluster. The other three haloes, which have been extracted from a single Lagrangian region, correspond to groups in the mass range $(2\text{--}6) \times 10^{13} M_\odot$. In the following, we will refer to these three structures as ‘group 1’, ‘group 2’ and ‘group 3’. In Table 1 we provide the main characteristics of the simulated structures.

We follow the technique originally presented by Katz & White (1993) to increase the mass resolution and to add short-wavelength modes within Lagrangian regions that contain the structures of interest. In these high-resolution regions, particles are split into a dark matter and a gaseous part, with the mass ratio reflecting the value of the cosmic baryon fraction. Force and mass resolution are then gradually degraded in the outer regions, so as to limit the computational cost, while providing a correct representation of the large-scale tidal field. The size of the regions selected at $z = 0$, to be resimulated at high resolution, typically corresponds to 10–20 Mpc in Lagrangian space, and is always chosen to be large enough that no low-resolution heavy particles contaminate the virial region of the simulated haloes.

In order to assess numerical effects, structures have been simulated at different mass and force resolutions. We fix three different mass resolutions, which correspond to $m_{\text{gas}} \simeq 2.5 \times 10^9 M_\odot$, $3.2 \times 10^8 M_\odot$ and $3.9 \times 10^7 M_\odot$ for the mass of the gas particles, respectively. In the following, the group runs with the smallest (intermediate) value of m_{gas} and the Virgo runs with the intermediate (largest) m_{gas} will be indicated as high-resolution (low-resolution) runs and labelled with HR (LR). We do not discuss Virgo runs with the smallest m_{gas} and group runs with the largest m_{gas} among this list of three mass resolutions. With these choices for the mass resolution, the HR runs resolve the virial regions of the simulated structures with a number of gas particles ranging from about 70 000 to about 185 000 (see Table 1). The redshift z_i at which initial conditions are generated is chosen such that the rms fluctuation in the density field of the high-resolution region is $\sigma = 0.1$ (on the scale of the smallest resolved masses). With this requirement, we have $z_i \simeq 65$. As for the choice of the softening scale for the computation of the gravitational force, we assume it to have a constant value in comoving units down to $z = 2$, and a constant value in physical units at later epochs. The corresponding values of the Plummer-equivalent softening scale at $z = 0$ are $\epsilon_{\text{pl}} = 10, 5$ and 2.5 kpc for the three different choices of m_{gas} . This choice has been dictated by the requirement of resolving haloes down to scales of about 1 per cent of their virial radii, so as to correctly follow the gas clumpiness and, therefore, to have convergent estimates of the X-ray luminosity (e.g. Borgani et al. 2002).

We show in Fig. 1 the gas density and entropy maps for the HR runs of the cluster and of the group regions at $z = 0$ for the runs including cooling and star formation (see below). In the entropy map of the Virgo cluster (lower left-hand panel), we note a tail of

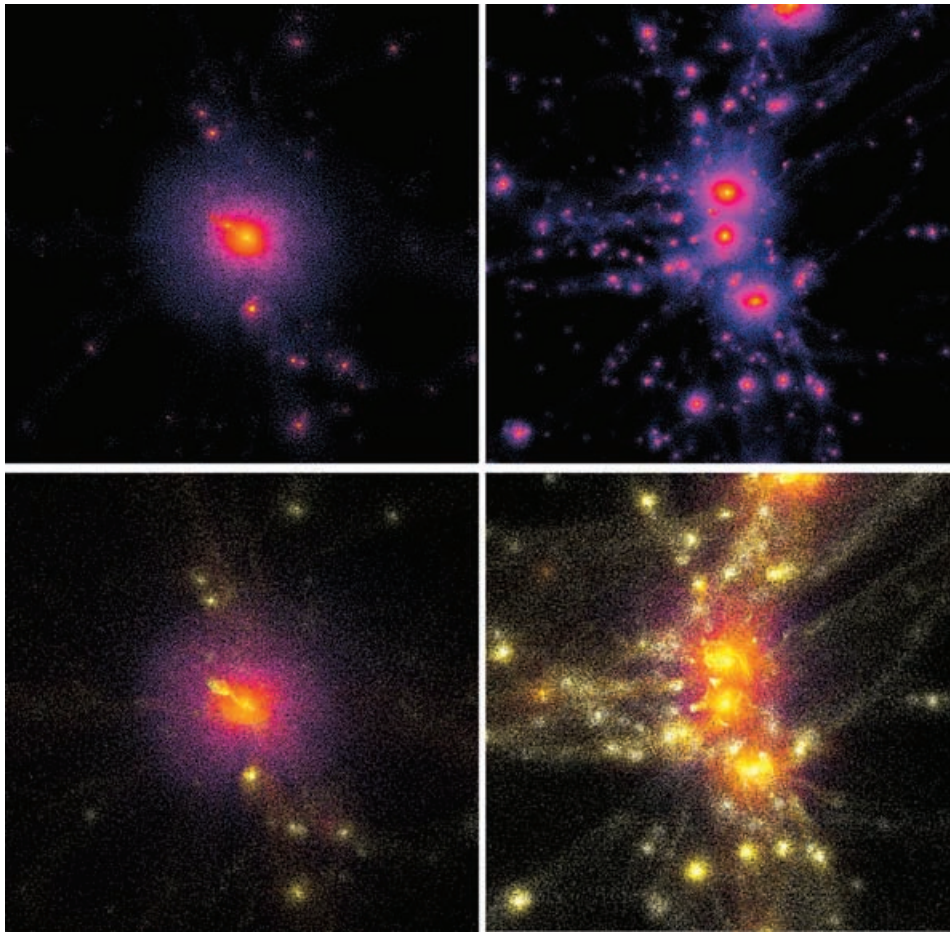


Figure 1. Maps of the gas density (upper panels) and of the gas entropy (lower panels) for the Virgo run (left-hand panels) and for the region containing the groups (right-hand panel), for the HR runs including cooling and star formation (see the text). The size of each box is 10 Mpc, so as to show the environment of the simulated systems. Brighter regions indicate higher gas density and lower entropy in the upper and lower panels, respectively.

low-entropy gas pointing toward the centre. This feature is generated by a merging subgroup, for which the gas has been tidally stripped during the first passage through the cluster virial region. The persistence of low entropy for this gas indicates that it has been only recently stripped and has still to thermalize within the cluster environment. As apparent from the gas-density map (upper left-hand panel), this merging subhalo gives rise only to a minor disturbance of the gas density, thus marginally disturbing the relaxed dynamical status of the cluster. As for the simulation of the region containing the three groups, we note that they are placed along a filamentary structure. Although they are still relatively isolated and separated from each other by a few virial radii, their motion shows that they are approaching each other and will merge to form a cluster-sized structure in a few Gyr. In general, these maps witness that a rich variety of structures, emerging when high resolution is achieved, are naturally expected to characterize the ICM, much like that shown by high-resolution *Chandra* observations.

3 COMPUTING THE COLLAPSED GAS FRACTION IN CLUSTER SIMULATIONS

3.1 Introducing radiative cooling

An important aspect when dealing with simulations that include cooling concerns the detailed scheme of SPH implementation. Most

standard implementations integrate the specific thermal energy as an independent variable, differing, however, in the detailed method used for symmetrizing the pairwise hydrodynamic forces between gas particle pairs, where either a simple arithmetic or a geometric mean form the most common choices (e.g. Weinberg, Hernquist & Katz 1997; Davé et al. 1999; White, Hernquist & Springel 2001). While these SPH implementations conserve energy and momentum, Springel & Hernquist (2002, SH02 hereafter) have shown that several of the commonly used SPH implementations are characterized by a spurious loss of specific entropy in strongly cooling regions, an effect which can be particularly severe at low resolution, and which is stronger when the geometrical scheme for hydrodynamical force symmetrization is adopted. This problem is essentially due to spurious coupling between cool dense particles, which should have virtually left the collisional phase, and neighbouring hot gas particles, which still belong to the diffuse phase. In order to avoid the resulting spurious overcooling, different techniques have been suggested by several authors (e.g. Pearce et al. 2001; Marri & White 2002).

SH02 proposed a new SPH implementation based on integrating the specific entropy as an independent thermodynamic variable, an approach which explicitly conserves entropy in non-shock regions. Using a variational principle to derive the SPH equations of motion, they also showed that this new formulation removes any ambiguity in the choice of symmetrization

and conserves energy, even when adaptive smoothing lengths are used.

Since one of the main purposes of this paper is to investigate the properties of gas cooling in galaxy clusters, we will study below by how much differences in the SPH implementation can change the resulting fraction of cold gas. Adopting the naming convention of SH02, we refer to a standard SPH implementation with geometric symmetrization as ‘geometrical’, and to one with arithmetic symmetrization as ‘arithmetic’, while the new formulation of SH02 will be referred to as ‘entropy-conserving’.

3.2 Introducing star formation

Star formation is introduced as an algorithm to remove dense cold gas particles from the SPH computation, treating them as collisionless ‘stars’. We follow the recipe originally proposed by KWH. According to this recipe, a gas particle is eligible to form stars if the following conditions are met: (i) a locally convergent flow, $\nabla \cdot \mathbf{v} < 0$; (ii) it is Jeans unstable, i.e. the locally determined sound crossing time is longer than the dynamical crossing time; (iii) the gas overdensity exceeds a critical overdensity value, $\delta_g > 55$; (iv) the local number density of hydrogen atoms $n_H > 0.1 \text{ cm}^{-3}$.

Once a particle is eligible to form stars, its star formation rate (SFR) is given by $d \ln \rho_g / dt = -c_*/t_g$, where t_g is the minimum between the local gas-dynamical time-scale, $t_{\text{dyn}} = (4\pi G \rho_g)^{-1/2}$, and the local cooling time-scale. We assumed $c_* = 0.1$ for the parameter regulating the rate of conversion of cold gas into stars, and verified with a low-resolution simulation of the Virgo cluster that basic results are left essentially unchanged by instead taking $c_* = 0.01$. A gas particle eligible for star formation is assumed to be gradually converted into a star particle, according to the above SFR. Instead of creating a new star particle for every star formation (SF) instance, each gas particle undergoing SF behaves in a ‘schizophrenic’ way, with its stellar part feeling only gravity (see, e.g., Mihos & Hernquist 1994). Once the SPH mass fraction decreases to 10 per cent, it is dissolved into SPH neighbours, thus leaving a purely stellar particle.

We also follow the recipe by KWH to compute the energy feedback from the SN associated with the star formation produced in the simulations. Assuming a Miller–Scalo (1979) initial mass function (IMF), we compute the number of stars with mass $> 8 M_\odot$, which we identify with instantaneously exploding SNe. After assuming that each SN releases 10^{51} erg, the resulting amount of energy per formed stellar mass turns out to be $7 \times 10^{48} \text{ erg } M_\odot^{-1}$. While the approximation of instantaneous explosion can be justified for type II SN, due to the short lifetime of their progenitor stars, it is not valid for type Ia SN, which have stellar progenitors of smaller masses and much longer lifetimes (e.g. Lia, Portinari & Carraro 2002; Pipino et al. 2002; Valdarnini 2002). The resulting feedback energy is assigned as thermal energy to the star-forming gas particles. This scheme for SN feedback is known to thermalize a negligible amount of energy in the diffuse medium, since it acts mostly on cold dense particles that rapidly radiate away the feedback energy as a consequence of their short cooling time. In the following, we show results based on including this scheme for SN feedback while bearing in mind that it causes only negligible differences compared with simulations that lack any stellar feedback. In Section 3.3 we shall discuss a different SN feedback scheme, based on the predictions of semi-analytical modelling of galaxy formation.

The effect of including star formation on the fraction of collapsed gas in the Virgo cluster run is shown in Fig. 2. Besides the population of collisionless star particles, we also define as belonging to

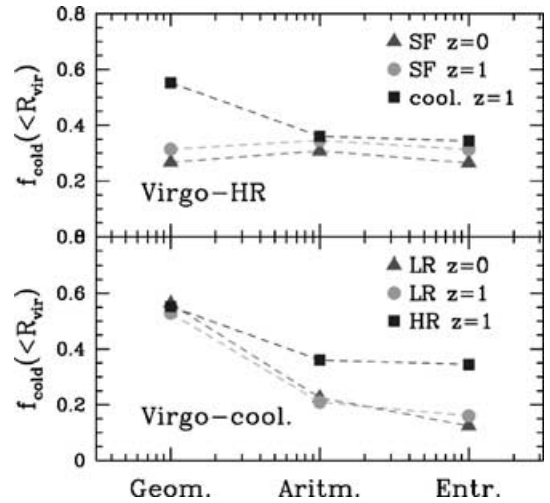


Figure 2. The fraction of collapsed gas within the virial radius for the Virgo run, for the three different schemes of SPH implementation. The lower panel refers to runs including cooling but not star formation. The upper panel shows the effect of introducing star formation for the HR runs.

the cold phase all the SPH particles that have an overdensity $\delta_{\text{gas}} > 500$ and a temperature $T < 3 \times 10^4 \text{ K}$ (see also Croft et al. 2001; Borgani et al. 2002). At $z = 1$, the star formation simulation produces $f_{\text{cold}} \simeq 25\text{--}35$ per cent collapsed gas, with a weak dependence on the integration scheme. However, in the cooling-only simulations, where collapsed gas is not converted to stars, the ‘geometric’ scheme leads to substantially larger values, indicating a numerical overcooling problem in this method. This effect is absent in the entropy-conserving scheme, which proves effective in suppressing spurious cooling in the absence of an explicit SF scheme. Note that f_{cold} is seen to slightly decrease at later epochs, which is as a consequence of a reduction of the rate at which cooling and star formation proceeds with respect to diffuse gas accretion.

In Fig. 3 we show the trend of f_{cold} against the emission-weighted temperature, which is defined here as

$$T_{\text{ew}} = \frac{\sum_i \rho_i T_i^{3/2}}{\sum_i \rho_i T_i^{1/2}}, \quad (1)$$

where ρ_i is the gas density carried by the i th SPH particle. This definition is valid only for bremsstrahlung emissivity, although final values of T_{ew} are left essentially unchanged if we account for the contribution from metal lines.

For the groups, we plot results for both the LR and the HR runs. The trend toward a higher f_{cold} in colder systems is a consequence

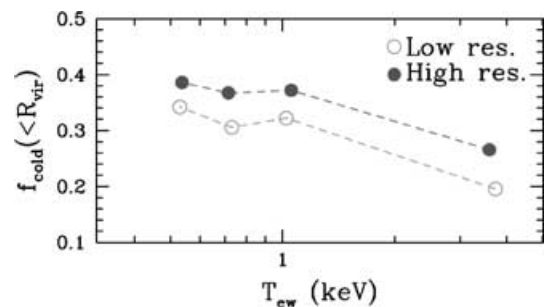


Figure 3. The fraction of cold gas as a function of the emission-weighted temperature, T_{ew} , of the simulated structures. Results at two different resolutions are shown for the simulations of the groups.

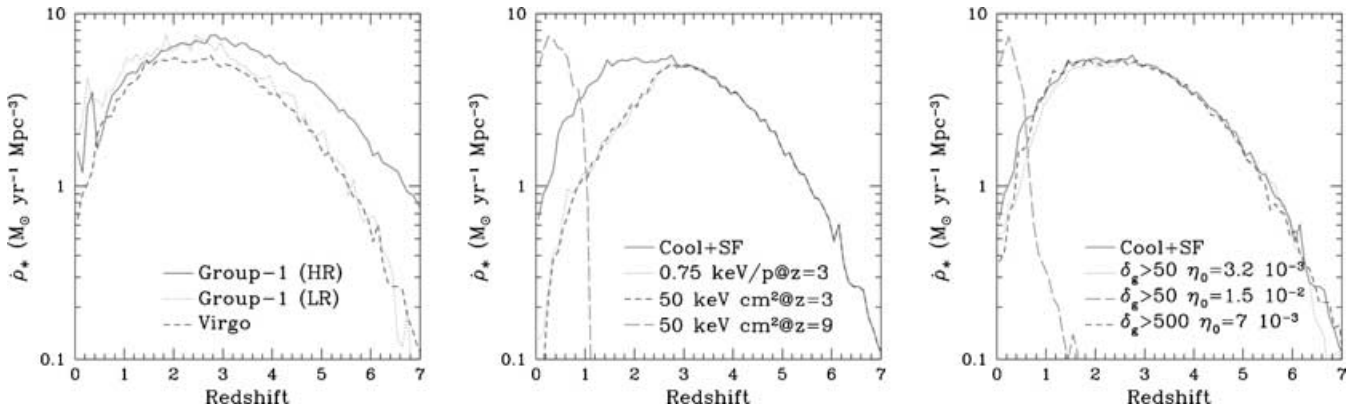


Figure 4. The density of the star formation rate, $\dot{\rho}_*(t)$, computed for the Lagrangian volume of the object corresponding to the $z = 0$ virial region of the simulated systems. Left-hand panel: $\dot{\rho}_*(t)$ for the Virgo simulation (dashed curve) and for both the LR and HR runs of group 1 (dotted and solid curves, respectively), when no extra heating is included. Central and right-hand panels: results for the Virgo cluster, simulated with impulsive heating and SAM-predicted SN heating, respectively.

of the shorter cooling times of the associated DM haloes, which makes cooling proceed faster in lower-mass systems. Apparently, increasing the resolution causes a ~ 20 per cent or a ~ 50 per cent increase of f_{cold} at the group and at the cluster scales, respectively. The effect of numerical resolution is also shown in the left-hand panel of Fig. 4. In this figure we plot the density of star formation rate within the virial region of the Virgo cluster and of the group 1. Once the same mass resolution is used for the simulation of these two structures, the resulting SFRs are quite similar. Increasing the resolution of the group simulation allows one to resolve smaller haloes forming at higher z , where additional star formation can take place. As a result, the peak in the SFR moves from $z \simeq 2$ to $z \simeq 3$ and then declines more gently, while recovering the same shape at lower redshift. Note that the integrated star formation rate is dominated by the contribution from these low redshifts, where most of the physical time is being spent. The resolution achieved in the HR runs is sufficient to resolve ‘galaxy’ haloes well below L_* . Therefore, we are confident that we are obtaining nearly converged estimates of the collapsed gas fraction, at least when the highest mass resolution is used. At the same time, our results should be considered as a warning on the interpretation of simulations that lack the resolution to adequately follow gas cooling.

In summary, our simulations demonstrate that cold fractions as large as $f_{\text{cold}} = 25\text{--}35$ per cent should be expected when radiative cooling and star formation are considered. These values are larger than the observed ~ 10 per cent fraction of cold gas in clusters (e.g. Balogh et al. 2001). This calls for the need to introduce a suitable scheme of non-gravitational energy injection, allowing a regulation of the runaway cooling process.

3.3 Introducing extra heating

The SN feedback recipe that we have discussed so far, where thermal energy is deposited into cold gas, does not produce any sizeable effect. In order to overcome this problem, many different schemes have been proposed. All of these schemes attempt to prevent feedback energy from being quickly radiated away, for example by suitably parametrizing ‘subgrid’ physics, such as the multiphase structure of the interstellar medium or galactic winds (e.g. Kay et al. 2000; Marri & White 2002; Springel & Hernquist 2002).

Here we present different phenomenological approaches for non-gravitational heating. Rather than predicting feedback from the star

Table 2. Prescriptions for non-gravitational heating. In column 1 we give the name of the runs. For the impulsive heating schemes we give: in column 2 the quantity that is modified by the heating; column 3 the heating redshift z_h . For the SAM-predicted SN feedback we give in column 2 the number of SN per unit M_\odot ; column 3 the limiting density contrast for the gas particles to be heated. Column 4 gives the mean specific energy assigned to the gas particles falling within R_{vir} by $z = 0$. The asterisks indicate those runs that have only been realized for the ‘Virgo’ cluster.

| Impulsive heating | | | |
|---------------------------|--|------------|------------------------|
| Name of run | Scheme | z_h | $E_h(<R_{\text{vir}})$ |
| S25-9* | $S_{\text{fl}} = 25 \text{ keV cm}^2$ | 9 | 0.5 |
| S50-9 | $S_{\text{fl}} = 50 \text{ keV cm}^2$ | 9 | 0.9 |
| S50-3 | $S_{\text{fl}} = 50 \text{ keV cm}^2$ | 3 | 0.8 |
| K75-3 | $E_h = 0.75 \text{ keV particle}^{-1}$ | 3 | 0.75 |
| SAM-predicted SN feedback | | | |
| Name of run | η_0 | δ_g | $E_h(<R_{\text{vir}})$ |
| SN03 _L | 3.2×10^{-3} | 50 | 0.15 |
| SN07 _L * | 7.0×10^{-3} | 50 | 0.32 |
| SN15 _L * | 1.5×10^{-2} | 50 | 0.43 |
| SN07 _H | 7.0×10^{-3} | 500 | 0.36 |

formation actually produced in the simulations, these schemes are designed to shed light on how much extra energy is required and how it should be distributed in redshift and as a function of the local gas density, to prevent overcooling and, at the same time, to reproduce X-ray observables of galaxy clusters and groups. A summary of the characteristics of the heating recipes that we explore here is provided in Table 2. In the rest of the paper we will present results based only on the high-resolution runs.

3.3.1 Impulsive heating

In our first class of heating schemes, we assume that all the energy is dumped into the diffuse baryons in an impulsive way, with a single heating episode occurring at some redshift z_h .

(a) Entropy floors $S_{\text{fl}} = 50 \text{ keV cm}^2$ at redshift $z_h = 9$ (S50-9 runs) and at $z_h = 3$ (S50-3 runs), and $S_{\text{fl}} = 25 \text{ keV cm}^2$ at $z_h = 9$. In this scheme, the entropy associated with each gas particle, $s = T/n_e^{2/3}$ (T , temperature in keV; n_e , electron number density in cm^{-3}) is either increased to the value S_{fl} if smaller than that, or otherwise left unchanged (see also Navarro et al. 1995; Bialek et al. 2001; BGW).

The choice of $z_h = 9$ corresponds to a heating epoch well before a substantial amount of gas in simulations cools and forms stars and, therefore, heavily suppresses star formation. The existence of a pristine SN generation (from the so-called Population III stars) has been invoked to account for the intergalactic medium (IGM) metal enrichment (e.g. Madau, Ferrara & Rees 2001). However, were this heating able to raise the entropy to the above levels, it would prevent the later formation of the Ly α forest, which is known to have about one order of magnitude lower entropy. Furthermore, the amount of heating energy would also correspond to too high production of heavy elements. For these reasons, we consider this choice for S_{II} to be motivated by the phenomenology of X-ray ICM properties alone, rather than by expectations from star formation processes at high redshift.

(b) A fixed amount of heating energy per particle, $E_h = 0.75$ keV particle $^{-1}$ at $z_h = 3$. This amount of energy is roughly the same as the average specific energy dumped by the S50-3 scheme within the halo virial radius (see Table 2). Therefore, it allows one to check for differences induced in the final results by distributing the same energy budget in a different way as a function of gas density. The $z_h = 3$ heating epoch is close to that at which the star formation rate within a protocluster region peaks (e.g. Menci & Cavaliere 2000; Bower et al. 2001; BGW). An energy budget $E_h \sim 0.6$ – 0.8 keV particle $^{-1}$ has also been suggested by Finoguenov et al. (2001a) to be consistent with the Si abundance detected in groups and clusters.

3.3.2 SAM-predicted SN feedback

This heating scheme is based on computing the star formation rate within clusters using a semi-analytic model (SAM) of galaxy formation (e.g. Kauffmann, White & Guiderdoni 1993; Somerville & Primack 1999; Cole et al. 2000 and references therein). Here we employ a variation of the scheme described by Menci & Cavaliere (2000, see also Bower et al. 2001), and we refer to their paper for a detailed description of the method, while we refer to BGW for further details on its implementation in cluster simulations.

The hierarchical merging of DM haloes is followed by means of the extended Press–Schechter formalism (e.g. Lacey & Cole 1993), while model parameters describing the gas physics, such as cooling, star formation and stellar feedback, are chosen so as to reproduce the observed properties of the local galaxy population, such as the Tully–Fisher relation, or optical luminosity functions and disc sizes (e.g. Poli et al. 2001). The model prediction we are interested in here is the integrated star formation history, $\dot{m}_*(z, M_0)$, of all the condensations which are incorporated into a structure of total mass M_0 by the present time. For a halo of size similar to our Virgo-like cluster, the SFR peaks at $z \simeq 4$ in this semi-analytic model, while it is $z \simeq 2.5$ – 3 for the group-sized haloes (see BGW, for a plot of the M_0 dependence of the cluster SFR).

The rate of total energy feedback released by type II SN is then computed as

$$\frac{dE_{\text{SN}}}{dt} = 10^{51} \text{ erg } \eta_0 \dot{m}_*(z, M_0), \quad (2)$$

where η_0 is the number of SNe per solar mass of formed stars. This value depends on the assumed initial mass function, and is obtained by integrating over the IMF for stellar masses $> 8 M_{\odot}$. In the following, we will use the values $\eta_0 = 3.2 \times 10^{-3} M_{\odot}^{-1}$, which follows from a Scalo IMF (Scalo 1956), $\eta_0 = 7 \times 10^{-3} M_{\odot}^{-1}$, from the Salpeter IMF (Salpeter 1955) and $\eta_0 = 1.5 \times 10^{-2} M_{\odot}^{-1}$, as an extreme case.

Since our simulations include cooling, radiative losses of SN energy do not need to be assumed a priori, rather they are self-consistently computed by the code. However, we need to specify the gas overdensity, δ_g , at which the SN heating energy is assigned to the gas. In the following we take $\delta_g = 50$ or 500 , and assume that E_{SN} is shared in equal parts among all the gas particles at overdensities larger than δ_g . The choice $\delta_g = 50$ corresponds to assuming that the virial region of the whole halo is heated and, therefore, that physical processes such as galactic winds, for example, are rather efficiently transferring energy to the IGM. Increasing δ_g implies two competitive effects: on one hand, it decreases the number of heated gas particles, therefore it increases the amount of extra energy assigned to each of them; on the other hand, the energy is assigned to denser particles, which have a shorter cooling time and, therefore, larger radiative losses.

3.4 The effect of extra heating on the cold fraction

As we have already discussed, introducing cooling causes a too large fraction of gas to be converted into stars. This is a well-known feature of hydrodynamical simulations, which has been widely discussed in the literature (e.g. Sugimoto & Ostriker 1998; BGW). Even worse, the runaway nature of the cooling process causes its efficiency to be highly sensitive to numerical resolution (see Fig. 3, see also Balogh et al. 2001). Therefore, one should be very cautious in the interpretation of results from simulations that do not resolve haloes with luminosity well below L_* .

In Fig. 5, we show the effect of the different heating schemes on the resulting cold fraction within the virial radius of our simulated structures. As expected, we find a decrease of f_{cold} when non-gravitational heating is included. However, the efficiency of this suppression of star formation does not exclusively depend on the amount of energy dumped. For instance, imposing an entropy floor of 50 keV cm^2 at $z_h = 9$ (left-hand panel of Fig. 5) is far more efficient than at $z_h = 3$. The reason for this is illustrated by the different patterns of SFR history, which we show in Fig. 4. The impulsive heating at $z_h = 3$ causes a suppression of the SFR at later epochs, but a fair number of stars are already in place at z_h (central panel of Fig. 4). Quite interestingly, the results for the two runs with heating at $z_h = 3$ produce quite similar SFR. This indicates that, once the heating epoch is fixed, the degree of SFR suppression depends only on the amount of heating energy, while being largely independent on its distribution as a function of the local gas density.

However, heating at $z = 9$ with a comparable amount of energy does not allow gas to reach high densities within DM haloes and to cool before $z \simeq 1$. Once cooling takes place, it converts less than 10 per cent of the gas into stars, within a short episode of star formation. The resulting SFR peaks at very low redshift, $z \simeq 0.3$, which is highly discrepant with observational determinations of the SFR history in clusters (e.g. Kodama & Bower 2001). Of course, this is not the only feature which rules out the picture of a strong heating occurring at such a high redshift. For instance, at $z = 0$, stars are all concentrated in one single object located at the centre, a cD-like galaxy, while no other galaxy-sized DM haloes contain significant amounts of collapsed gas.

As for the SN heating (right-hand panel of Fig. 4), suppressing the star fraction below the 10 per cent level requires a high, probably unrealistic value for η_0 . Also, taking $\eta_0 = 1.5 \times 10^{-2} M_{\odot}^{-1}$ generates an implausible SFR history, resembling that found for the runs based on setting the entropy floor at $z_h = 9$: the large amount of extra heating at high redshift prevents the occurrence of star formation down to $z \simeq 1.5$. Taking η_0 in the range 3 – 7×10^{-3} predicts more

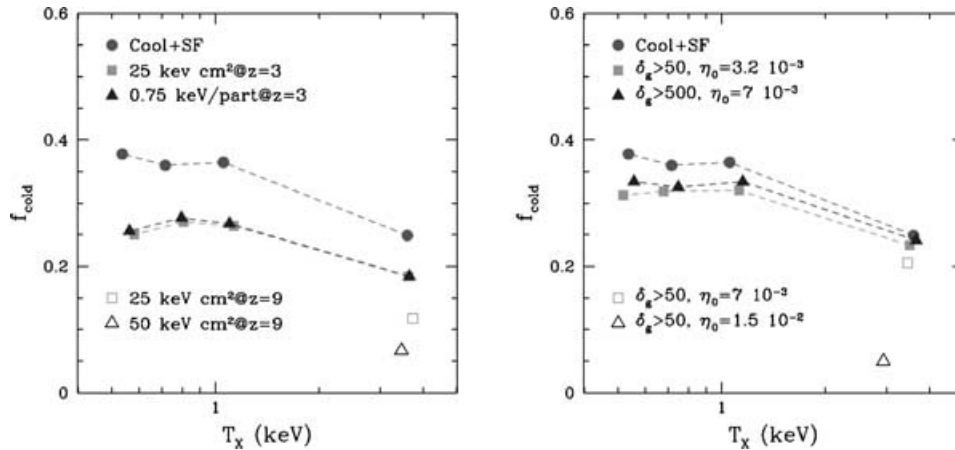


Figure 5. The fraction of cold gas within the virial region of the simulated structures at $z = 0$. The left- and right-hand panels show the effect of impulsive heating and of SAM-predicted SN feedback, respectively.

realistic SFRs, but it is not able to suppress f_{cold} below the $\simeq 20$ per cent level.

A general conclusion of our analysis is that heating schemes producing plausible SFR histories are not efficient in suppressing the fraction of cold gas below the 20 and 25 per cent values at the cluster and group scales, respectively. In contrast, a more efficient suppression is obtained by preventing gas from cooling at high redshift, at the expense of delaying star formation to unreasonably low redshifts.

4 X-RAY PROPERTIES OF SIMULATED CLUSTERS

4.1 The entropy of the ICM

Measurements of the excess entropy in central regions of poor clusters and groups are considered to provide direct evidence for the lack of self-similarity of the ICM properties (e.g. Ponman et al. 1999; Finoguenov et al. 2002a). In a separate paper (Finoguenov et al. 2002b), a self-consistent comparison is realized between the entropy properties of the simulations with impulsive heating, that we present here, and the observational data for groups and clusters by Finoguenov et al. (2002a). The main result of this comparison is that, although cooling and star formation tend to somewhat increase entropy in central cluster regions, they still fall short in producing the entropy excess which is observed at the group scale. While pre-heating at $z_h = 3$ is shown to increase the entropy to the observed values, runs with $z_h = 9$ are characterized by a low entropy level in central regions of clusters and groups.

Instead of attempting any further comparison with observations, we want to discuss here the dynamical reasons for such a behaviour. To this end, we show in Fig. 6 the effect of cooling and non-gravitational heating on the entropy profiles for our whole set of ‘Virgo’ simulations. As expected, when cooling and SF are included, low-entropy gas is selectively removed in central cluster regions, thus inducing a flattening of the profile. This is explicitly shown in Fig. 7: while the run including only gravitational heating has a population of high-density low-entropy gas particles, such particles are removed from the diffuse phase once cooling and star formation are introduced. This result is consistent with the expectation from analytical arguments based on the comparison between the cooling time-scale and the typical cluster age (e.g. Voit et al. 2002; Wu &

Xue 2002). The inclusion of extra heating has a non-trivial effect on the efficiency of cooling in removing particles from the lower left-hand side of the S - δ_g phase diagram. For instance, imposing the same entropy floor at $z_h = 9$ and at $z_h = 3$ has quite different effects on the entropy pattern (see the lower panels of Fig. 7). Heating at $z_h = 9$ has the effect of increasing the cooling time for most of the gas particles, so as to allow star formation to take place only quite recently (see Fig. 4). The increased time-scale for cooling causes this process to proceed in a more gradual way. For this reason, the entropy of gas particles undergoing cooling decreases slowly, thus making their removal from the hot diffuse phase less efficient.

4.2 The luminosity–temperature and luminosity–mass relations

The slope of the L_X - T relation also provides important observational evidence for the lack of self-similar behaviour of the ICM. Since the first measurements of ICM temperatures for sizeable sets of clusters, it has been recognized that $L_X \propto T^\alpha$ with $\alpha \simeq 3$, although with a considerable scatter (e.g. White, Jones & Forman 1997 and references therein). Better quality observations established that a significant contribution to this scatter is associated with the different strength of cooling flows detected in different clusters. Either excluding clusters with pronounced signatures of cooling flows or correcting for their effect (e.g. Allen & Fabian 1998; Markevitch 1998; Arnaud & Evrard 1999; Ettori et al. 2002) results in a much tighter L_X - T relation, albeit still with a rather steep slope. At the same time, hints have also been found for a further steepening of this relation at $T \lesssim 1$ keV (e.g. Helsdon & Ponman 2000 and references therein), possibly indicating that the mechanism responsible for the L_X - T scaling should act in a different way for clusters and groups.

Simulations that allow for non-gravitational heating (e.g. Bialek et al. 2001; BGW) and radiative cooling (e.g. Pearce et al. 2001; Davé et al. 2002; Muanwong et al. 2002) have been shown to be able to account for the observed L_X - T relation. However, a sometimes overlooked issue in determining the X-ray luminosity of clusters in simulations concerns the contribution of metal lines to the emissivity. While this contribution is negligible above 2 keV, it becomes relevant at the scale of groups. For instance, neglecting the contribution from line emissivity for an ICM enriched to a metallicity of $Z = 0.3 Z_\odot$ leads to an underestimate of the X-ray luminosity by

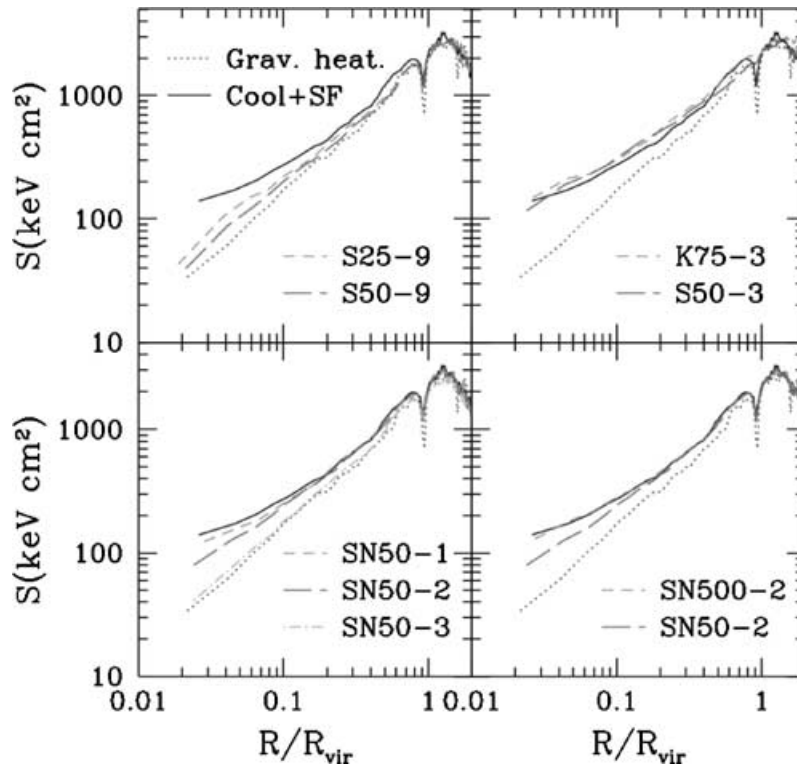


Figure 6. The entropy profiles of the ‘Virgo’ cluster simulations. The upper panels show the effect of impulsive heating at $z = 9$ (on the left) and $z = 3$ (on the right), while the lower panels show the effect of SN feedback from the SAM-predicted SFR history, after changing η_0 (on the left) and the density threshold for gas heating (on the right). For reference, the entropy profiles for the run with gravitational heating and for the run including only cooling and star formation are shown in all the panels with the dotted and the solid lines, respectively.

almost 50 per cent at 1 keV, and by more than a factor of 2 at 0.5 keV (e.g. BGW).

A correct procedure would require simulations that include a treatment of metal enrichment and a self-consistent estimate of the contribution of line cooling to the X-ray emissivity. However, only preliminary attempts have been realized so far to include the treatment of ICM metal enrichment from SN ejecta (Lia, Portinari & Carraro 2002; Valdarnini 2002). Pearce et al. (2001) include the contribution of metals to the cooling function adopted in their simulation by assuming $Z = 0.3 Z_{\odot}$ at the present epoch, linearly decreasing with time towards the past. Davé et al. (2002) did not include the metal contribution in their cooling function, but estimated X-ray luminosities by assuming a phenomenological relation between metal abundance and temperature of the galaxy system. However, while the ICM metallicity at the scale of rich clusters is quite well established from observations, the situation is less clear for poor clusters and groups (e.g. Davis, Mulchaey & Mushotzky 1999; Renzini 2000 and references therein).

The cooling function used in our simulations assumes zero metallicity, but we compute the X-ray luminosity by adding to the bremsstrahlung emissivity the contribution from lines for a $Z = 0.3 Z_{\odot}$ plasma. This represents a reasonable approximation as long as gas spends most of the time at low metallicity, being enriched to high metallicity only recently. Owing to the uncertainties connected to these assumptions, the reliability of L_X values at $T \lesssim 1$ keV is unclear, however. Precise predictions will require a fully self-consistent treatment of metal enrichment of the ICM from star formation activity.

In Fig. 8, we show the profiles of emissivity (energy released per unit time and unit volume) for the different Virgo runs. As expected,

including only cooling and star formation has the effect of flattening the profiles in the central cluster regions as a consequence of gas removal from the hot phase. When extra heating is included, the profiles change according to the amount of gas left at relatively low entropy in the central cluster regions. For instance, the fairly large population of low-entropy particles in the run with $S_{fl} = 50$ keV cm^2 at $z_h = 9$ (see Fig. 7) is responsible for the spike in the X-ray emissivity. In the same way, the efficient removal of low-entropy gas for the run where an entropy floor was imposed at $z_h = 3$ explains the flattening of the luminosity profile in the central cluster region. These results confirm the existence of a non-trivial interplay between the effects of cooling and extra heating. In some cases, one reaches the apparently paradoxical conclusion that combining heating and cooling increases the X-ray luminosity, although their separate effects are that of suppressing L_X .

Fig. 9 shows the comparison between the simulated and the observed L_X - T relation for clusters and groups. As expected, cooling causes a sizeable suppression of the X-ray luminosity. At the same time, the emission-weighted temperature is increased as a consequence of the steepening of the temperature profiles in the central halo regions (see below). While the mere introduction of cooling and star formation brings the ‘Virgo’ cluster into agreement with observations, the simulated groups are somewhat overluminous with respect to data. The inclusion of pre-heating at $z_h = 3$ has a smaller effect on the Virgo cluster, consistent with the result from the luminosity profile, while it further suppresses L_X at the scale of groups. A similar result is also found for the runs with SAM-predicted SN feedback.

Quite interestingly, the L_X value for group 2 in the runs with no extra heating appears to be systematically in excess with respect

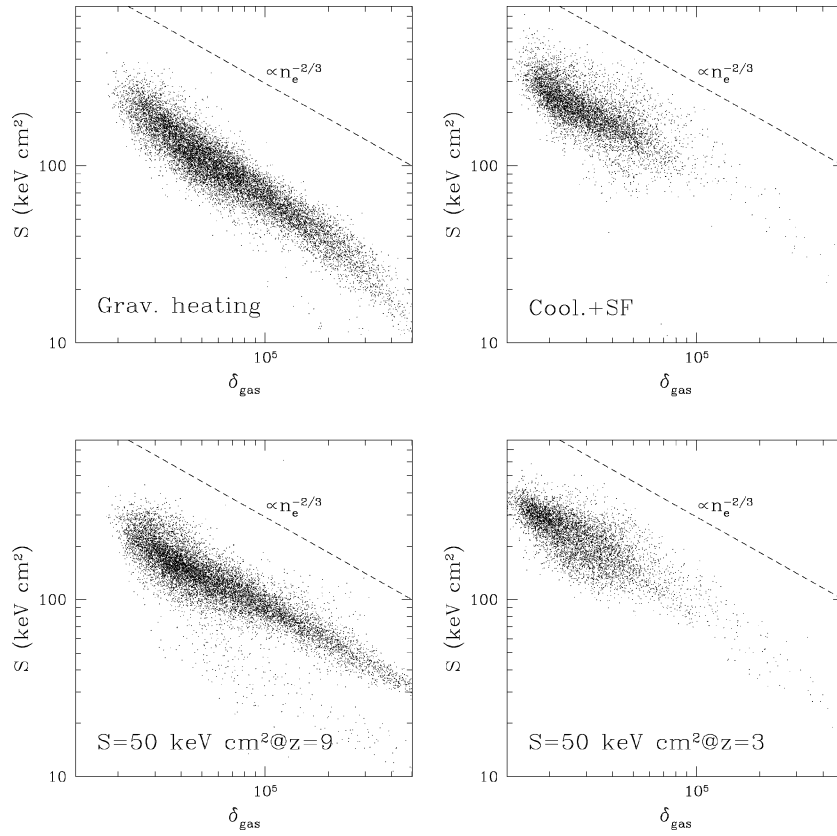


Figure 7. The entropy–overdensity phase diagram for the gas particles falling within $0.1 R_{\text{vir}}$ at $z = 0$, for different runs of the ‘Virgo’ cluster. In each panel, the dashed line shows the scaling $S \propto n_e^{-2/3}$ expected for isothermal gas.

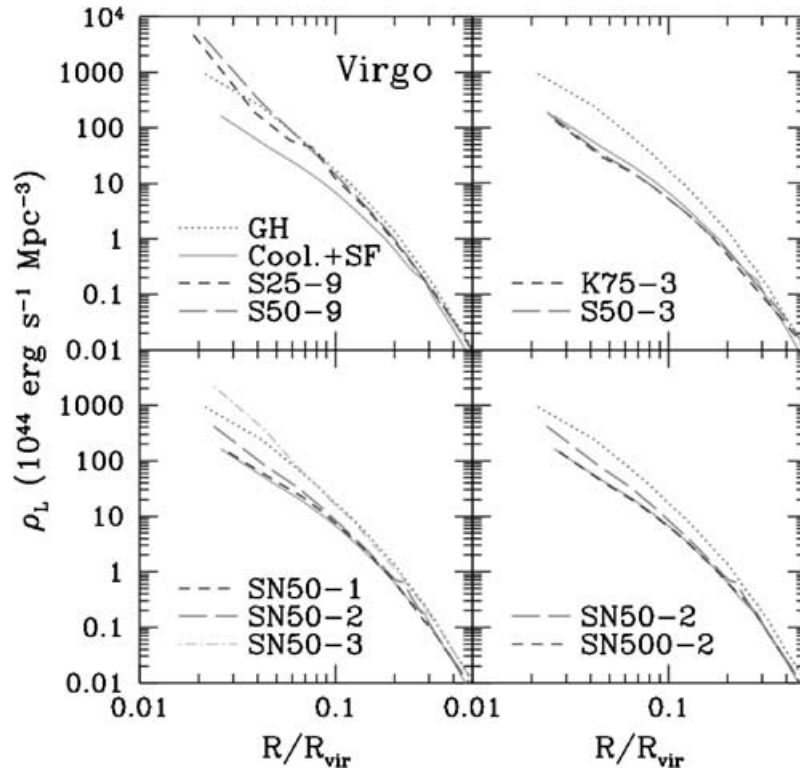


Figure 8. The profiles of X-ray luminosity density for the ‘Virgo’ runs. The sequence of panels is the same as in Fig. 6.

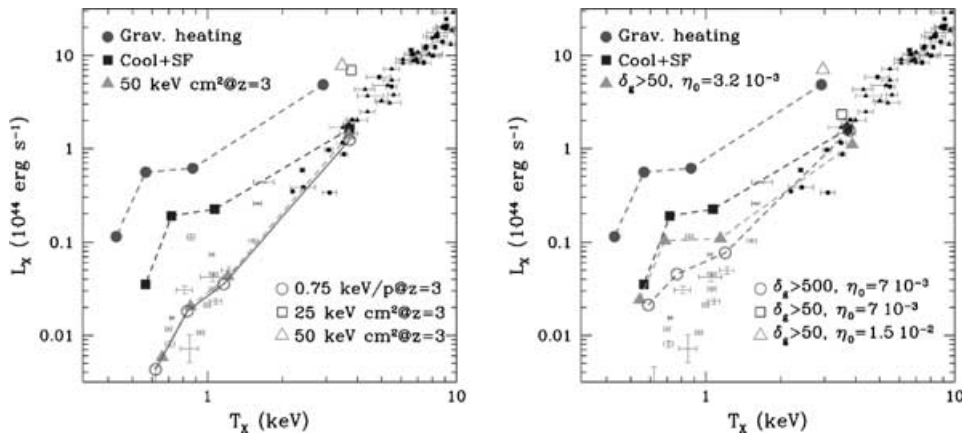


Figure 9. The relation between bolometric luminosity and emission-weighted temperature for the simulations and for observational data at $z = 0$. The right- and the left-hand panels are for the effects of impulsive heating and SN feedback, respectively. Data points at the cluster scale are from Markevitch (1988, small triangles) and from Arnaud & Evrard (1999, small squares) while data for groups (crosses) are from Helsdon & Ponman (2000).

to that inferred from the L_X – T scaling of the other three simulated structures. This deviation is due to the occurrence of a recent merger shock in the group 2 run, which produced a sudden increase in the X-ray emission. When extra heating is included, its effect is that of decreasing the strength of the shock, thus also reducing the jump in luminosity.

A similar constraint is provided by the relation between X-ray luminosity and mass. Reiprich & Böhringer (2002) have estimated this relation by applying the equation of hydrostatic equilibrium to a fairly large ensemble of clusters and groups, under the assumption of isothermal gas. They used ICM temperatures based on *ASCA* data, in combination with *ROSAT* PSPC data for the surface brightness profile. Ettori et al. (2002) used the better quality data from *Beppo-SAX* observations to resolve the temperature profiles for a smaller ensemble of clusters. Although the analysis by Ettori et al. explicitly includes temperature gradients when solving the equation of hydrostatic equilibrium, it is restricted to clusters with $T \gtrsim 3$ keV, thus hotter than those simulated here. For this reason, here we compare our simulation results with the data of Reiprich & Böhringer (see Fig. 10). In this analysis, the cluster masses, M_{500} , are computed within the radius encompassing an average density $\bar{\rho} = 500\rho_{\text{crit}}$, while observed luminosities are provided in the 0.1–2.4 keV *ROSAT* energy band. We use the MEKAL spectral model to correct bolometric luminosities from simulations by assuming $Z = 0.3 Z_{\odot}$ for the global ICM metallicity. Consistent with the results from the analysis of the L_X – T relation, we find that the runs with heating at $z_h = 3$ and that with SN feedback, based on a Salpeter IMF, are able to follow the steep slope of the observed $L_{0.1-2.4}$ – M_{500} relation.

In principle, the L_X – T and the L_X – M relations do not provide independent information, since masses are estimated using temperature data. Still, both relations are obtained using significantly different observational data sets and analysis procedures. Therefore, the fact that the same simulations are able to account for both scalings lends support to the robustness of our results and indicates that our conclusions are not affected by observational biases or systematics.

Owing to the uncertainties mentioned above in modelling the luminosities of groups, it appears prudent not to make strong claims about how much extra heating is needed to reproduce the observations. Overall, we note that all the runs that produce a delayed star formation, such as those with $z_h = 9$ and that with SN-feedback and large $\eta_0 = 1.5 \times 10^{-2} M_{\odot}^{-1}$ (see Fig. 4), are quite inefficient

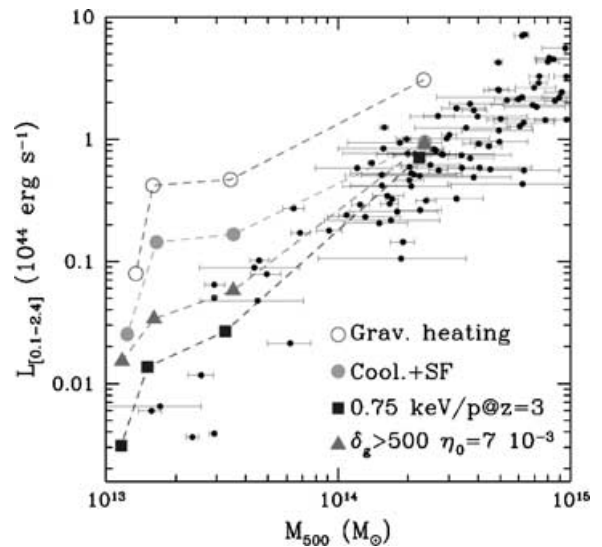


Figure 10. Comparison of simulations and observational results for the relation between X-ray luminosity in the 0.1–2.4 keV energy band and the mass at an overdensity of $\bar{\rho}/\rho_{\text{crit}} = 500$. Small circles with error bars are the observational data points from Reiprich & Böhringer (2002).

in suppressing L_X . In contrast, runs with pre-heating at $z_h = 3$ or with SN feedback combined with more reasonable values for η_0 succeed in accounting for the steep slopes of the L_X – T and L_X – M relations.

Having warned about the reliability of the emissivity modelling for gas at $T < 1$ keV, a word of caution should also be given on the reliability of the interpretation of current observational data. Estimating the temperature and the luminosity for small groups from pre-*Chandra* and pre-*XMM* data is not a trivial task, mostly due to the difficulty of separating the contribution of the diffuse intragroup medium from that of member galaxies, and of detecting X-ray emission out to a significant fraction of the virial radius (see, e.g., Mulchaey 2000 for a review on the X-ray properties of groups). The situation is likely to improve as newer and better quality data are accumulated, although we will probably have to wait for a few more years before a critical amount of *Chandra* and *Newton-XMM* observations of groups will be available.

4.3 The mass–temperature relation

Under the assumptions of spherical symmetry and an isothermal gas distribution, the condition of hydrostatic equilibrium predicts a precise relationship between the virial mass of a cluster and its temperature: $k_B T = 1.38 \beta^{-1} M_{15}^{2/3} [\Omega_m \Delta_{\text{vir}}(z)]^{1/3} (1+z)$ keV for a gas of primordial composition, with M_{15} being the virial mass in units of $10^{15} h^{-1} M_\odot$ and Δ_{vir} being the ratio between the virial density and the average cosmic matter density at redshift z . Under the above assumptions, the β parameter gives the ratio between the specific kinetic energy of dark matter particles and the thermal energy of the gas. Simulations including only gravitational heating demonstrated that this relation is reproduced quite well, with $\beta \simeq 1$ – 1.2 (e.g. Evrard et al. 1996; Bryan & Norman 1998; Frenk et al. 1999; BGW). For these reasons, the M – T relation has been considered for several years as a fairly robust prediction of hydrostatic equilibrium: gas temperature, unlike X-ray emissivity, is primarily determined by the action of gravity and, as such, depends on global cluster properties and only weakly on the local structure of the ICM.

However, data based on *ASCA* and *ROSAT* observations show an M – T relation that is about 40 per cent lower than predicted (Horner, Mushotzky & Scharf 1999; Nevalainen, Markevitch & Forman 1999; Finoguenov et al. 2001b), a result that has been confirmed by *Beppo-SAX* (Ettori et al. 2002) and *Chandra* (Allen et al. 2001) data for relatively hot systems ($T \gtrsim 4$ keV).

Non-gravitational heating could be naively expected to solve this discrepancy by increasing the ICM temperature at fixed cluster mass. However, BGW have shown that for a broad class of pre-heating models similar to those discussed here the M – T relation is left almost unchanged by the injection of extra energy (cf. also Lin et al. 2002). In fact, as long as gas has time after being heated to settle back into hydrostatic equilibrium within the gravitational potential well, its temperature is mainly determined by the amount of collapsed dark matter, which is unaffected by the heating process.

An alternative explanation for the observed low amplitude of the M – T relation, based on the effect of radiative cooling, has been shown by Thomas et al. (2002) to be much more promising. In this case, gas left in the diffuse phase flows towards the central cluster region, where it is compressed, thus increasing its temperature. As a result, the overall mass-weighted temperature remains almost unchanged, but the emission-weighted temperature increases significantly. Our results, as shown in Fig. 11, actually confirm this picture and generalize it to a large range of schemes for extra heating: while

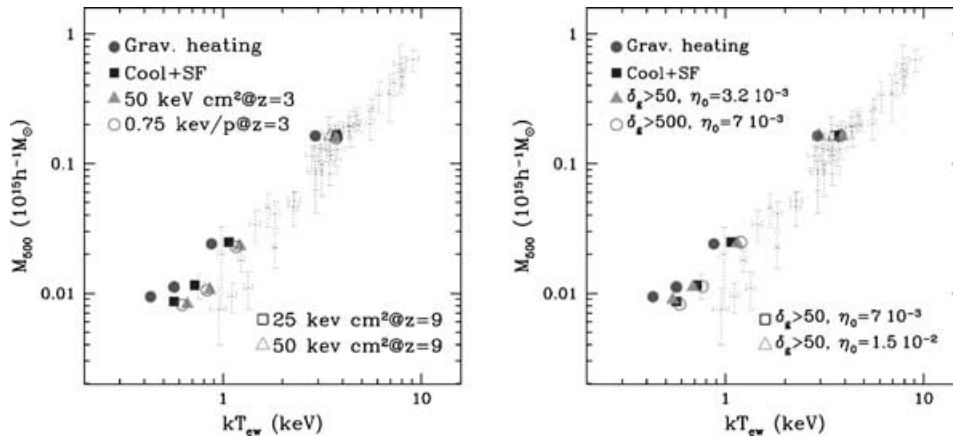


Figure 11. The relation between the mass at overdensity $\rho/\rho_{\text{crit}} = 500$ and the emission-weighted temperature. The right- and the left-hand panels are for the effects of impulsive heating and SN feedback, respectively. Data points are from Finoguenov et al. (2001b).

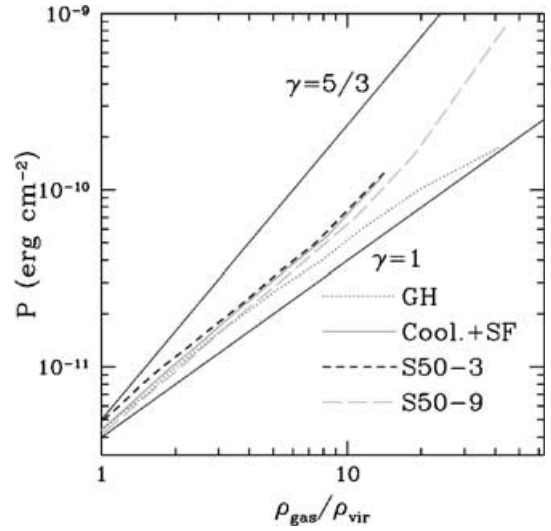


Figure 12. The relation between gas pressure (cgs units) and density (in units of the average total density within the virial radius), computed within spherical shells. The two thin solid lines correspond to effective polytropic indices $\gamma = d \log P / d \log \rho_{\text{gas}} = 1$ (isothermal model) and $\gamma = \frac{5}{3}$ (adiabatic model).

the value of M_{500} is left unchanged by the cooling/heating processes, T_{ew} increases as a consequence of the temperature increase in the central cluster regions.

In order to better understand the effect of cooling on the central temperature structure of the ICM, we plot in Fig. 12 the gas pressure, $P = \rho_{\text{gas}} k_B T / (\mu m_p)$, as a function of gas density for the simulations of the ‘Virgo’ cluster. We introduce here the effective polytropic index $\gamma = d \log P / d \log \rho_{\text{gas}}$ to describe the run of pressure as a function of gas density. In the external cluster region the gas is characterized by $\gamma \gtrsim 1$, thus consistent with the slowly outward-declining temperature profiles, almost independent of the presence of cooling and extra heating. However, cooling leads to a loss of pressure in central high-density regions. As cooling partially removes low-entropy gas from the diffuse phase, gas of higher entropy flows in from more external regions. As long as this gas has a sufficiently long cooling time, its entropy is conserved and the gas is adiabatically compressed during the inflow. In this regime, the effective polytropic index increases towards $\gamma = \frac{5}{3}$, thus indicating an

adiabatic behaviour of the ICM. This result is essentially independent of whether gas is pre-heated. The only effect of imposing an entropy floor at $z_h = 9$ is that of making the cooling process more gradual. This allows a larger amount of gas to remain in the diffuse phase, so as to reach a higher density and pressure in central regions (see also Fig. 8).

4.4 The temperature profiles

The way in which cooling acts in reconciling the observed and the simulated M - T relations implies that temperature profiles should steepen in central cluster regions. From an observational viewpoint, the possibility of realizing spatially resolved spectroscopy has recently opened the possibility of determining temperature profiles for fairly large samples of clusters. Interestingly, observations based on the *ASCA* (e.g. Markevitch et al. 1998) and *Beppo-SAX* (De Grandi & Molendi 2002) satellites show *declining* temperature profiles in the outer regions, at cluster-centric distances $\gtrsim 0.2$ – $0.3R_{\text{vir}}$ (cf. also Irwin & Bregman 2000). This behaviour is generally reproduced by simulations that do not include cooling (e.g. BGW). Furthermore, both *Beppo-SAX* (De Grandi & Molendi 2002), *Chandra* (e.g. Etti et al. 2002; Allen et al. 2001; Johnstone et al. 2002) and *XMM* (e.g. Tamura et al. 2001) data for fairly hot systems, $T_X \gtrsim 4$ keV, show temperature profiles declining towards the very central regions of clusters, thus indicating the presence of cooling cores. This behaviour is grossly at variance with respect to that found for the ‘Virgo’ runs, as reported in Fig. 13: the only case where a somewhat declining profile is produced is that with gravitational heating, while cooling always gives rise to steeply increasing profiles with no evidence for any decline, independent of the presence of extra heating.

A more comprehensive comparison with the observations would require simulations to be realized for a set of clusters with higher

temperature. On the other hand, our simulated Virgo cluster has been chosen as a fairly relaxed system. Therefore, as long as observations suggest profiles to be universal for such systems (Allen et al. 2001), such a discrepancy should be taken quite seriously. A steepening of the temperature profiles caused by cooling has already been noticed by Lewis et al. (2000), Muanwong et al. (2002) and Valdarnini (2002). The temperature profiles in Fig. 13 generalize this also result in the presence of a variety of extra-heating mechanisms.

We also note that the steep temperature profiles predicted by simulations are also at variance with respect to those predicted by the semi-analytical model for ICM heating/cooling by Voit et al. (2002). A detailed comparison between the predictions of semi-analytical models and simulations is beyond the scope of this paper. However, a full understanding of the physical processes taking place in the ICM will only be obtained if the reasons for such differences can be understood and eventually sorted out.

If the discrepancy between observed and simulated temperature profiles is confirmed, it may indicate that we are missing some basic physical mechanism that affects the thermal properties of the gas in the high-density cooling regions. For instance, thermal conduction has been advocated by some authors as a mechanism that, in combination with central heating, may regulate gas cooling (e.g. Voigt et al. 2002) while providing acceptable temperature profiles for a suitable choice of the conductivity parameter (e.g. Zakamska & Narayan 2002; Ruszkowski & Begelman 2002). In this scenario, one expects the outer layers to heat gas in the innermost regions, so as to increase its cooling time, allowing it to stay in the diffuse phase at a relatively low temperature. However, the detection of sharp features in the temperature map of several clusters, as observed by the *Chandra* satellite, led some authors to suggest that thermal conduction is suppressed in the ICM (e.g. Etti & Fabian 2000). Magnetic fields are naturally expected to produce such a suppression (e.g. Sarazin 1988). Still, it is not clear whether this mechanism can act

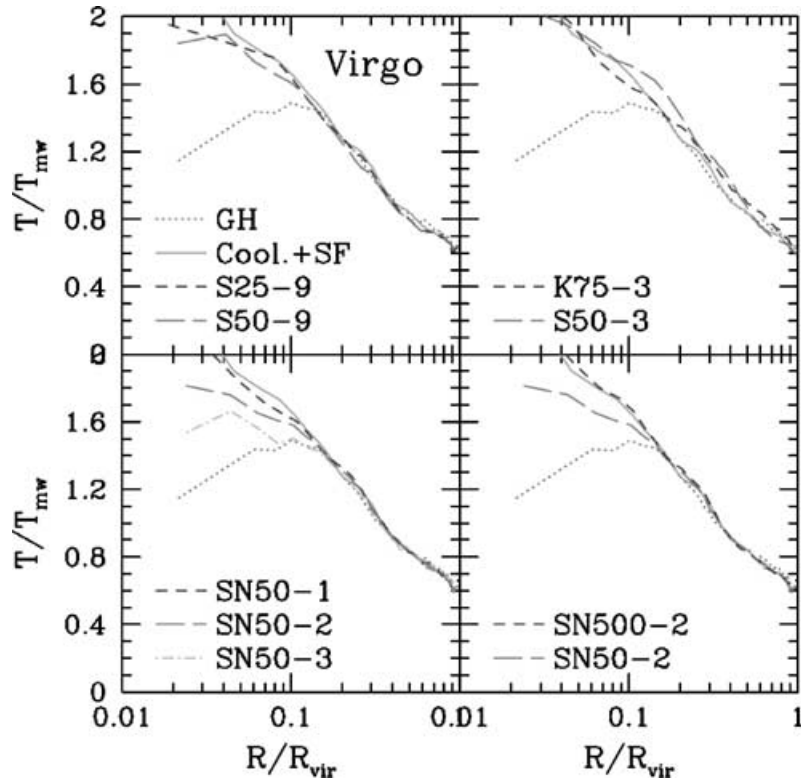


Figure 13. Temperature profiles of the ‘Virgo’ runs, in units of the mass-weighted temperature. The sequence of panels is the same as in Fig. 6.

in a ubiquitous way inside clusters or whether the turbulence associated with the presence of magnetic fields is actually able to maintain a relatively efficient thermal conduction (e.g. Narayan & Medvedev 2001).

5 DISCUSSION AND CONCLUSIONS

We presented results from high-resolution tree+SPH simulations of a moderately poor ‘Virgo’-like cluster and of three group-sized haloes, including the effects of radiative cooling and non-gravitational gas heating. The numerical accuracy reached in these simulations was aimed at following in detail the pattern of gas cooling and its effect on the X-ray properties of groups and clusters of galaxies. The main results that we obtained can be summarized as follows.

(i) Including cooling and star formation causes a fraction $f_* \simeq 0.25$ of baryons to be converted into a collisionless ‘stellar’ phase in the Virgo cluster and $f_* \simeq 0.35\text{--}0.40$ in the simulated groups. Given the sensitivity of cooling on numerical resolution, it is likely that the result for the ‘Virgo’ run should still be interpreted as a lower limit on f_* .

(ii) The cold fraction is reduced by including non-gravitational heating. The degree to which overcooling is suppressed depends not only on the amount of feedback energy, but also on the redshift and on the gas overdensity at which it is released into the diffuse medium. For instance, heating at $z_h = 9$ is very efficient in decreasing f_* below the 10 per cent level, at the expense of delaying the bulk of star formation to $z \lesssim 1$. A more realistic star formation history, peaking at $z \simeq 3$, consistently requires that most of the non-gravitational heating takes place at a similar redshift, with at least 20 per cent of the baryons still being converted into stars.

(iii) Heating at $z_h = 3$ with $E_h \simeq 0.75$ keV particle⁻¹ is shown to produce scalings of X-ray luminosity, mass and entropy versus temperature that agree in general with observational data. This result holds independent of whether an equal amount of energy is assigned to all gas particles or whether an entropy floor is created. A similar agreement is also found for the SAM-predicted SN feedback, once realistic models for the IMF are used. Both, heating at $z_h = 9$, or using an IMF that produces a large number of SNe, are not efficient in suppressing the X-ray luminosity, which is a consequence of the fairly large amount of gas that, while avoiding cooling, is concentrated in central cluster regions.

(iv) Including cooling and star formation increases the ICM temperature in the central regions. While this helps in reconciling simulations with the observed $M\text{--}T$ relation, it steepens the temperature profiles, which show no evidence for any decline at small cluster-centric distances. This result, which holds independent of the scheme for non-gravitational heating, is discrepant with recent observations.

Over the last year or so, different groups have presented simulations aimed at studying the effect of radiative cooling and feedback on the X-ray properties of the ICM. Most of these studies are based on simulations that follow the gas hydrodynamics within the full volume of a cosmological box (e.g. Muanwong et al. 2002; Davé et al. 2002; Kay et al. 2002). One common result of these simulations, which agrees with what we find in our analysis, is that the effect of cooling is able to alleviate or even solve the discrepancy between simulated and observed X-ray scaling properties of clusters and groups, but the fraction of baryons converted into stars is too large. To remedy this problem, Muanwong et al. (2002) pre-heated the gas by adding 1.5 keV of thermal energy to all the gas particles

at $z_h = 4$. As a result, they found that the cold fraction in groups and clusters decreased from 15 to 0.4 per cent, which is somewhat smaller than the values found in our simulations. Kay et al. (2002) implemented a feedback mechanism in their simulations, which accounts for the rate of both type Ia and type II SNe. By assuming an energetics twice as large as that provided by standard supernova computations, they were able to reproduce the observed X-ray scaling properties, while obtaining that only 3 per cent of the gas is converted into stars. The main limitation of this type of simulation is that one is restricted to relatively poor numerical resolution in order to limit the computational cost. For instance, the simulations by Muanwong et al. (2002) have a mass resolution that is about one order of magnitude worse than that of our ‘Virgo’ runs and almost two orders of magnitude worse than that of our group runs. A better mass resolution within a smaller box was used by Kay et al. (2002), for which the mass of gas particles are a factor of 2.8 and 22 smaller than for our Virgo and group runs, respectively.

The results that we presented in Section 3 demonstrate that the cooling efficiency is quite sensitive to mass resolution. For this reason, one has to be careful in drawing conclusions concerning overcooling and how it is suppressed by extra heating, in the presence of limited numerical resolution. In fact, our simulations demonstrate that the two main problems caused by the introduction of radiative cooling, namely the overproduction of stars and the steeply increasing temperature profiles in central cluster regions, may not be easily solved by the introduction of non-gravitational heating.

Does this imply that none of our heating schemes are a realistic approximation to what happens in real clusters? The energy release in all of these schemes fails, although to different degrees, to faithfully follow the simulated rate of star production. A realistic scheme for SN feedback should dump thermal energy with a rate that accurately follows the star formation rate, properly accounting for the typical lifetimes of different stellar populations. Furthermore, our schemes for energy release demonstrate that for feedback to have a sizeable effect on the ICM thermodynamics, it has to act in a non-local way, so as to assign most of the energy to gas particles that have a sufficiently long cooling time. Such non-local feedback mechanisms may arise from AGN activity, cosmic rays or galactic winds, for example.

While further work is clearly needed to study such feedback mechanisms self-consistently in simulations, a better understanding is also required as to whether optical/X-ray data really implies a stellar fraction as small as $\lesssim 10$ per cent within clusters and groups. Balogh et al. (2001) used the 2MASS results on the K -band luminosity function by Cole et al. (2001) to estimate the cosmic fraction of baryons converted into stars. After assuming a Kennicutt IMF (Kennicutt 1983), they find $f_* \simeq 0.05$ for our choice of Ω_m and h , and argued that no much evidence exists for f_* to increase inside clusters or to depend on the cluster mass (cf. also Bryan 2000). However, this estimate of the cosmic value of f_* increases by about a factor of 2 if a Salpeter IMF (Salpeter 1955) is used instead. Furthermore, it is worth reminding the reader that the estimate inside clusters relies to some degree on extrapolation. For instance, Balogh et al. (2001) obtained the stellar mass in clusters from the B -band luminosity data by Roussel, Sadat & Blanchard (2000), using $M/L_B = 4.5$, and correcting for undetected galaxies by extrapolating the luminosity function to the faint end slope. It is clear that a more robust determination of f_* in clusters should rather rely on K - or H -band luminosity, which is more directly related to stellar mass (e.g. Gavazzi & Scodreggio 1996), rather than to B -band luminosity for which the conversion to stellar mass is quite sensitive to galaxy morphology. More recently, Huang et al. (2003) used the

Hawaii AAO *K*-band redshift survey to estimate the *K*-band luminosity function in the local Universe. They found that the *K*-band luminosity density is twice as large as that from 2MASS, thus implying twice as large an f_* value. In light of this discussion, an f_* value somewhat larger than 10 per cent, possibly as large as 20 per cent, may still be viable at present, which would tend to alleviate the problem of ICM overcooling.

As for the temperature profile, our results indicate that the discrepancy between observations and simulations is unlikely to be solved by the inclusion of feedback mechanisms that are similar to those explored here. If this is the case, it would demonstrate that our simulations are missing some basic physical mechanisms. For instance, as we discussed, thermal conduction has been proposed to be an important effect in clusters. Another piece of physics which is currently missing from most simulation work is the effect of magnetic fields (e.g. Dolag, Bartelmann & Lesch 2002). Their introduction might give rise to non-trivial structures in the gas distribution if they can locally suppress thermal conduction, or if they provide a non-thermal contribution to the gas pressure.

There is little doubt that including such more complex physics will represent a significant, non-trivial challenge for cluster simulations of the next generation. Most of the processes involved require both a rather sophisticated numerical method and a treatment of subgrid physics. Still, the inclusion of more physics in numerical codes is mandatory if the reliability and the predictive power of cluster simulations want to keep pace with the increasing quality of observational data.

ACKNOWLEDGMENTS

Simulations were run at the CINECA Supercomputing Centre, with CPU time being provided by a grant from the National Institute for Astrophysics (INAF), at the Computing Centre of the Astronomical Observatory of Catania and at the Computing Center of the University of Trieste. We wish to thank Hans Bühringer, Alexis Finoguenov, Fabio Governato, Paolo Tozzi and Xian-Ping Wu for enlightening discussions.

REFERENCES

- Allen S.W., Fabian A.C., 1998, *MNRAS*, 297, 63
 Allen S.W., Schmidt R.W., Fabian A.C., 2001, *MNRAS*, 328, L37
 Arnaud M., Evrard A.E., 1999, *MNRAS*, 305, 631
 Babul A., Balogh M.L., Lewis G.F., Poole G.B., 2002, *MNRAS*, 330, 329
 Balogh M.L., Babul A., Patton D.R., 1999, *MNRAS*, 307, 463
 Balogh M.L., Pearce F.R., Bower R.G., Kay S.T., 2001, *MNRAS*, 326, 1228
 Bialek J.J., Evrard A.E., Mohr J.J., 2001, *ApJ*, 555, 597
 Borgani S. et al., 2001a, *ApJ*, 561, 13
 Borgani S., Governato F., Wadsley J., Menci N., Tozzi P., Lake G., Quinn T., Stadel J., 2001b, *ApJ*, 559, L71
 Borgani S., Governato F., Wadsley J., Menci N., Tozzi P., Quinn T., Stadel J., Lake G., 2002, *MNRAS*, 336, 409 (BGW)
 Bower R.G., 1997, *MNRAS*, 288, 355
 Bower R.G., Benson A.J., Bough C.L., Cole S., Frenk C.S., Lacey C.G., 2001, *MNRAS*, 325, 497
 Brighenti F., Mathews W.G., 2001, *ApJ*, 553, 103
 Bryan G.L., 2000, *ApJ*, 544, L1
 Bryan G.L., Norman M.L., 1998, *ApJ*, 495, 80
 Burles S., Tytler D., 1998, *Space Sci. Rev.*, 84, 65
 Cavaliere A., Menci N., Tozzi P., 1998, *ApJ*, 501, 493
 Cavaliere A., Lapi A., Menci N., 2002, *ApJ*, 581, L1
 Cole S., Lacey C., Baugh C., Frenk C., 2000, *MNRAS*, 319, 168
 Cole S. et al., 2001, *MNRAS*, 326, 255
 Croft R.A.C., Di Matteo T., Davé R., Hernquist L., Katz N., Fardal M.A., Weinberg D.H., 2001, *ApJ*, 557, 67
 Davé R., Hernquist L., Katz N., Weinberg D.H., 1999, *ApJ*, 511, 521
 Davé R., Katz N., Weinberg D.H., 2002, *ApJ*, 579, 23
 Davis D.S., Mulchaey J.S., Mushotzky R.F., 1999, *ApJ*, 511, 34
 De Grandi S., Molendi S., 2002, *ApJ*, 567, 163
 Dolag K., Bartelmann M., Lesch H., 2002, *A&A*, 387, 383
 Eke V.R., Cole S., Frenk C.S., Henry P.J., 1998a, *MNRAS*, 298, 1145
 Eke V.R., Navarro J., Frenk C.S., 1998b, *ApJ*, 503, 569
 Ettori S., 2002, *MNRAS*, 323, L1
 Ettori S., De Grandi S., Molendi S., 2002, *A&A*, 391, 841
 Ettori S., Fabian A.C., 2000, *MNRAS*, 317, L57
 Ettori S., Fabian A.C., Allen S.W., Johnstone R.M., 2002, *MNRAS*, 331, 635
 Evrard A.E., Henry J.P., 1991, *ApJ*, 383, 95
 Evrard A.E., Metzler C.R., Navarro J.F., 1996, *ApJ*, 469, 494
 Fairley B.W., Jones L.R., Scharf C., Ebeling H., Perlman E., Horner D., Wegner G., Malkan M., 2000, *MNRAS*, 315, 669
 Finoguenov A., Arnaud M., David L.P., 2001a, *ApJ*, 555, 191
 Finoguenov A., Reiprich T.H., Böhringer H., 2001b, *A&A*, 369, 479
 Finoguenov A., Jones C., Böhringer H., Ponman T.J., 2002, *ApJ*, 578, 74
 Finoguenov A., Borgani S., Tornatore L., Böhringer H., 2003, *A&A*, 398, L35
 Frenk C.S. et al., 1999, *ApJ*, 525, 554
 Gavazzi G., Scodreggio M., 1996, *A&A*, 312, L29
 Haardt F., Madau P., 1996, *ApJ*, 461, 20
 Helsdon S.F., Ponman T.J., 2000, *MNRAS*, 315, 356
 Holden B., Stanford S.A., Rosati P., Squires G.K., Tozzi P., Eisenhardt P., Elston R., 2002, *AJ*, 124, 33
 Horner D.J., Mushotzky R.F., Scharf C.A., 1999, *ApJ*, 520, 78
 Huang J.-S., Glazebrook K., Cowie L.L., Tinney C., 2003, *ApJ*, 584, 203
 Irwin J.A., Bregman J.N., 2000, *ApJ*, 538, 543
 Johnstone R.M., Allen S.W., Fabian A.C., Sanders J.S., 2002, *MNRAS*, 336, 299
 Kaiser N., 1986, *MNRAS*, 222, 323
 Kaiser N., 1991, *ApJ*, 383, 104
 Katz N., White S.D.M., 1993, *ApJ*, 412, 455
 Katz N., Weinberg D.H., Hernquist L., 1996, *ApJS*, 105, 19 (KWH)
 Kauffmann G., White S.D.M., Guiderdoni B., 1993, *MNRAS*, 264, 201
 Kay S.T., Pearce F.R., Jenkins A., Frenk C.S., White S.D.M., Thomas P.A., 2000, *MNRAS*, 316, 374
 Kay S.T., Thomas P.A., Theuns T., 2002, *MNRAS*, submitted (astro-ph/0210560)
 Kennicutt R.C., 1983, *ApJ*, 272, 54
 Kodama T., Bower R.G., 2001, *MNRAS*, 321, 18
 Kravtsov A.V., Yepes G., 2000, *MNRAS*, 318, 227
 Lacey C., Cole S., 1993, *MNRAS*, 262, 627
 Lewis G.F., Babul A., Katz N., Quinn T., Hernquist L., Weinberg D.H., 2000, *ApJ*, 623, 644
 Lia C., Portinari L., Carraro G., 2002, *MNRAS*, 330, 821
 Lin K.-Y., Lin L., Woo T.-P., Tseng Y.-H., Chiueh T., 2002, preprint (astro-ph/0210323)
 Lloyd-Davies E.J., Ponman T.J., Cannon D.B., 2000, *MNRAS*, 315, 689
 Madau P., Ferrara A., Rees M.J., 2001, *ApJ*, 555, 92
 Markevitch M., 1998, *ApJ*, 504, 27
 Markevitch M., Forman W.R., Sarazin C.L., Vikhlinin A., 1998, *ApJ*, 503, 77
 Marri S., White S.D.M., 2002, *MNRAS*, submitted (astro-ph/0207448)
 McNamara B.R. et al., 2000, *ApJ*, 534, L135
 Menci N., Cavaliere A., 2000, *MNRAS*, 311, 50
 Mihos J.C., Hernquist L., 1994, *ApJ*, 437, 47
 Miller G.E., Scalzo J.M., 1979, *ApJS*, 41, 513
 Muanwong O., Thomas P.A., Kay S.T., Pearce F.R., 2002, *MNRAS*, 336, 527
 Mulchaey J.S., 2000, *ARA&A*, 38, 289
 Mushotzky R.F., Scharf C.A., 1997, *ApJ*, 482, L13
 Narayan R., Medvedev M.V., 2001, *ApJ*, 562, 129

- Nath B.B., Roychowdhury S., 2002, *MNRAS*, 333, 145
- Navarro J.F., Frenk C.S., White S.D.M., 1995, *MNRAS*, 275, 720
- Nevalainen J., Markevitch M., Forman W., 1999, *ApJ*, 526, 1
- Nevalainen J., Markevitch M., Forman W.R., 2000, *ApJ*, 532, 694
- Novicki M.C., Sornig M., Henry J.P., 2002, *AJ*, 124, 2413
- Oh S.-P., Benson A.J., 2002, *MNRAS*, submitted (astro-ph/0212309)
- Pearce F.R., Jenkins A., Frenk C.S., White S.D.M., Thomas P.A., Couchman H.M.P., Peacock J.A., Efstathiou G., 2001, *MNRAS*, 326, 649
- Pierpaoli E., Borgani S., Scott D., White M., 2002, *MNRAS*, in press (astro-ph/0210567)
- Pipino A., Matteucci F., Borgani S., Biviano A., 2002, *New Astron.*, 7, 227
- Poli F., Menci N., Giallongo E., Fontana A., Cristiani S., D'Odorico S., 2001, *ApJ*, 551, L45
- Ponman T.J., Bourner P.D.J., Ebeling H., Böhringer H., 1996, 293, 690
- Ponman T.J., Cannon D.B., Navarro J.F., 1999, *Nat.*, 397, 135
- Reichart D.E., Nichol R.C., Castander F.J., Burke D.J., Romer A.K., Holden B.P., Collins C.A., Ulmer M.P., 1999, *ApJ*, 518, 521
- Reiprich T.H., Böhringer H., 2002, *ApJ*, 567, 716
- Renzini A., 1997, *ApJ*, 488, 35
- Renzini A., 2000, in Plionis M., Georgantopoulos I., eds, *Large Scale Structure in the X-ray Universe*. Atlantisciences, Paris, p. 103
- Roussel H., Sadat R., Blanchard A., 2000, *A&A*, 361, 429
- Ruskowski M., Begelman M.C., 2002, *ApJ*, 581, 223
- Salpeter E.E., 1955, *ApJ*, 121, 161
- Sarazin C., 1988, *X-ray Emission from Clusters of Galaxies*. Cambridge Univ. Press, Cambridge
- Scalo J.M., 1956, *Fund. Cosm. Phys.*, 11, 1
- Somerville R.S., Primack J.R., 1999, *MNRAS*, 310, 1087
- Springel V., Hernquist L., 2002, *MNRAS*, 333, 649 (SH02)
- Springel V., Yoshida N., White S.D.M., 2001, *New Astron.*, 6, 79
- Suginohara T., Ostriker J.P., 1998, *ApJ*, 507, 16
- Tamura T. et al., 2001, *A&A*, 365, L87
- Thomas P.A., Muanwong O., Kay S.T., Liddle A.R., 2002, *MNRAS*, 330, L48
- Tozzi P., Norman C., 2001, *ApJ*, 546, 63
- Valageas P., Silk J., 1999, *A&A*, 350, 725
- Valdarnini R., 2002, *MNRAS*, 339, 1117
- Vikhlinin A., VanSpeybroeck L., Markevitch M., Forman W.R., Grego L., 2002, *ApJ*, 578, L107
- Voigt L.M., Schmidt R.W., Fabian A.C., Allen S.W., Johnstone R.M., 2002, *MNRAS*, 335, L7
- Voit G.M., Bryan G.L., Balogh M.L., Bower R.G., 2002, *ApJ*, 576, 601
- Weinberg D.H., Hernquist L., Katz N., 1997, *ApJ*, 477, 8
- White D.A., Jones C., Forman W., 1997, *MNRAS*, 292, 419
- White M., Hernquist L., Springel V., 2001, *ApJ*, 550, L129
- Wu K.K.S., Fabian A.C., Nulsen P.E.J., 2000, *MNRAS*, 318, 889
- Wu X.-P., Xue Y.-J., 2002, *ApJ*, 569, 112
- Yoshida N., Stoehr F., Springel V., White S.D.M., 2002, *MNRAS*, 335, 762
- Zamaska N.L., Narayan R., 2003, *ApJ*, 582, 162

This paper has been typeset from a \TeX/L\AA\TeX file prepared by the author.